HEN-308/1988
16-12-88

FORWARD-BACKWARD MULTIPLICITY CORRELATIONS IN π^+p K^+p and pp COLLISIONS AT 250 GeV/c

NA22 Collaboration

Aachen-Antwerp/Brussels-Berlin (Zeuthen)-Helsinki-Krakow-
Moscow-Nijmegen-Rio de Janeiro-Serpukhov-Warsaw-Yerevan

V.V. AIVAZYAN[a], I.V. AJINENKO[b], Yu.A. BELOKOPYTOV[b], P.C. BOSETTI[h], H. BÖTTCHER[c], F. BOTTERWECK[d], P.V. CHLIAPNIKOV[b], F. CRIJNS[d], A. DE ROECK[e1], E.A. DE WOLF[e2], Th. DRIEVER[d], K. DZIUNIKOWSKA[f], A. ESKREYS[f], W. FRIEBEL[c], Z.C. GARUTCHAVA[b3], V.G. GAVRJUSEV[g], H. GRAESSLER[h], P. van HAL[d4], T. HAUPT[d5], W. KITTEL[d], S.S. MEGRABYAN[a], F. MEIJERS[d6], A.B. MICHALOWSKA[e], V.I. NIKOLAENKO[b], L.C.S. OLIVEIRA[i], K. OLKIEWICZ[f], L.P. PETROVIKH[b], E. RIIPINEN[j], V.M. RONJIN[b], A.M. RYBIN[b], H.M.T. SAARIKKO[j], W. SCHMITZ[h], L. SCHOLTEN[d7], R. SCHULTE[h], O.G. TCHIKILEV[b], L.A. TIKHONOVA[g], A.G. TOMARADZE[b3], V.A. UVAROV[b], F. VERBEURE[e], R. WISCHNEWSKI[c], A. WRÓBLEWSKI[k], S.A. ZOTKIN[g].

[a] Institute of Physics, SU-375036 Yerevan, USSR
[b] Institute for High Energy Physics, SU-142284 Serpukhov, USSR
[c] Institut für Hochenergiephysik der Akademie der Wissenschaften der DDR, DDR-1615 Berlin-Zeuthen, German Dem. Rep.
[d] University of Nijmegen and NIKHEF-H, NL-6525 ED Nijmegen, The Netherlands
[e] Universitaire Instelling Antwerpen, B-2610 Wilrijk and Inter-University Institute for High Energies, VUB/ULB, B-1050 Brussels, Belgium
[f] Institute of Physics and Nuclear Techniques of the Academy of Mining and Metallurgy and Institute of Nuclear Physics[8], PL-30055 Krakow, Poland
[g] Moscow State University, SU-117234 Moscow, USSR
[h] III. Physikalisches Institut B[9], RWTH, D-5100 Aachen, Fed. Rep. Germany
[i] Centro Brasileiro de Pesquisas Fisicas, 22290 Rio de Janeiro, Brazil
[j] Department of High Energy Physics, Helsinki University, SF-00170 Helsinki, Finland
[k] University of Warsaw and Institute of Nuclear Problems[8], PL-00681 Warsaw, Poland

ABSTRACT:

Forward-backward multiplicity correlations in π^+p, K^+p and pp collisions at 250 GeV/c ($\sqrt{s}$=22 GeV) are given for all charges and for the different charge combinations. The correlations are found to be caused predominantly by centrally produced particles. It is demonstrated that this result is in agreement with observations at the ISR and the CERN $p\bar{p}$- Collider. The results are compared to expectations from LUND, DPM and FRITIOF Monte Carlo models and a geometrical picture relating correlations in hadron-hadron collisions to e^+e^- data in terms of impact parameters is tested.

[redacted]

[1] Onderzoeker IIKW, Brussels, Belgium
[2] Bevoegdverklaard Navorser NFWO, Belgium
[3] Visitor from Inst. of High Energy Physics of Tbilisi State University, SU-380086 Tbilisi, USSR
[4] Now with Ericsson Telecommunicatie B.V., Rijen, The Netherlands
[5] On leave from Institute of Nuclear Physics, Krakow
[6] Now at CERN, Geneva, Switzerland
[7] Now with PANDATA, Rijswijk, The Netherlands
[8] Partially supported by grants from CPBP 01.06 and 01.09
[9] Partially funded by the German Federal Minister for Research and Technology (BMFT) under the contract number 053AC41P

1. INTRODUCTION

Production mechanisms at the parton level, coupled with the fragmentation into hadrons, lead to correlations between the final hadrons. Of fundamental interest are the correlations between the numbers of (charged) particles produced into, respectively, the forward and the backward cms hemisphere of a collision, the so-called forward and backward multiplicities n_F and n_B. Together with the full multiplicity distribution, the forward-backward (F-B) multiplicity correlation provides a first critical test of any model for hadron production and represents a useful tool for the study of the energy dependence and the comparison of different types of collision.

In hadron-hadron collisions clear evidence exists for strong F-B multiplicity correlations at high energies. For pp and $p\bar{p}$ collisions, for which the data are most abundant [1,2], the correlation strength increases logarithmically with energy, over a wide energy interval ($10 \leq \sqrt{s} \leq 900$ GeV). At the ISR and at the CERN $p\bar{p}$ Collider, it was found that the correlations are not only restricted to particles with a short distance in rapidity space, but also extend to particles with much wider rapidity separation [1d,2]. Several attempts have been made, to explain these correlations in the framework of different one and multi-string models [3]. Results have also been fitted by models with random emission of clusters along the rapidity axis [2,4]. However, the exact dynamical origin of these correlations still seems unclear.

The few existing meson-proton data [5-8] come essentially from lower energies and seem to follow the trend of the $pp(p\bar{p})$-data [9].

In contrast to hh collisions, such dynamical F-B multiplicity correlations are absent or small in e^+e^- annihilation [10] up to the highest energies so far reached at PETRA ($\sqrt{s}$=43.6 GeV). Results from the EMC-collaboration [11] indicate the absence of F-B correlations in μp-collisions within the W-interval of 4 to 20 GeV ($W = \sqrt{s}$). This seems also to be true for νp and $\bar{\nu} p$ reactions [12]. This would be expected from independent fragmentation of the final state, in e^+e^- annihilation essentially one quark-antiquark pair, in lepton-nucleon collisions one quark-diquark system.

The hadronic interaction, containing already 5 or 6 valence quarks in the initial state, is much more complicated. In addition to beam- and target-fragmentation, the bulk of the particles is produced in the central region. F-B correlations may, therefore, mainly be due to particles produced in the central region kinematically increasing with energy.

In this paper we report on measurements of the charged hadron F-B multiplicity correlations in π^+p, K^+p and pp reactions at a centre of mass energy $\sqrt{s}$=22 GeV.

In Sect. 2 we describe the experimental procedure and the selection of the data samples. In Sect. 3.1 we present F-B correlations in total phase space and compare these to other experiments and to Monte Carlo model calculations. In Sect. 3.2 we study definite charge combinations, in Sect. 4 we concentrate the analysis on central and off-central rapidity intervals. In Sect. 5 we try to interpret our results within the framework of a simple geometrical picture [13]. Finally, in Sect. 6 we summarize the main results.

2. THE DATA SAMPLE

The NA22 experiment has been performed at the CERN SPS with the European Hybrid Spectrometer (EHS), using the H_2 filled Rapid Cycling Bubble Chamber (RCBC) as an active vertex detector. The set-up was exposed to a 250 GeV/c tagged positive, meson enriched beam. In data taking, a minimum bias interaction trigger was used. The experimental set-up and the trigger conditions are described in ref. [14], where also details can be found pertaining to the topological cross sections and the general charge multiplicity distribution for our π^+p, K^+p and pp samples.

Charged particle tracks are reconstructed over the full solid angle from measurements in the bubble chamber and from hits in wire- and drift-chambers of the two lever arm magnetic spectrometer. The average momentum resolution $\langle \Delta p/p \rangle$ varies from a maximum of 2.5% at 30 GeV/c to 1.5% above 100 GeV/c. Events are accepted when topology and charge balance are correct, all tracks are reconstructed with $\Delta p/p < 0.25$ and no electron is detected among the secondary tracks.

It has been argued [15] that in a comparison of charge multiplicities in hh, lh and e^+e^- collisions non-diffractive hh events have to be used. We, therefore, restrict the analysis to the non-(single)-diffractive samples. These are defined by excluding low multiplicity events ($n \leq 6$ charged tracks) with at least one positive particle having Feynman $|x_F| > 0.88$. After application of these cuts, our sample consists of 53.000

π^+p, 22.000 K^+p and 3.900 pp collisions. This corresponds to 80% of the final π^+p and 100% of the K^+p and pp samples.

In determining the multiplicity in the forward and backward c.m. hemispheres separately, special care has to be devoted to the question of "spill-over". Due to the fact that an unidentified particle (proton or kaon) has been assigned the wrong mass (π mass), a backward going proton or kaon could falsely appear as a forward going pion. The effect has been studied in detail by making use of the large particle identification capacity of the EHS [16] as well as by means of Monte Carlo simulations. It turns out that this effect is small at our energies, if the ionization- and stopping track information in the bubble chamber is used for slow particles. At this stage, ionization information is used for the full K^+p and pp samples and for 23% of the π^+p sample, while stopping track information is available for the full sample. A correction for the migration in y due to the possible misidentification of the remaining tracks is applied from the Monte Carlo study.

3. CORRELATIONS IN TOTAL PHASE SPACE

To examine the correlations between particles produced in the forward ($x_F > 0$) and backward ($x_F < 0$) cms hemispheres, one investigates the average multiplicity in one hemishere as a function of the multiplicity in the opposite hemisphere. It has been noted already earlier [1d] that this relationship is linear.

If one denotes by $\langle n_B(n_F)\rangle$ the average multiplicity of charged particles produced in the backward hemisphere for a given multiplicity n_F of charged particles in the forward hemisphere, the correlation can be described by the formula

$$\langle n_B(n_F)\rangle = a_B + b_B \cdot n_F \qquad (1a)$$

or vice versa, with corresponding notation,

$$\langle n_F(n_B)\rangle = a_F + b_F \cdot n_B \quad . \qquad (1b)$$

The slope parameters b_B, b_F are a measure of the correlation strength between the multiplicity in the forward and backward hemispheres. For symmetric systems, such as e^+e^-, pp and $p\bar{p}$, $b_F = b_B$ must, of course, hold for an unbiased sample.

3.1 All Charged Particles

In Fig.1 we present the overall correlation $\langle n_B(n_F)\rangle$ for all charged particles produced in non-diffractive π^+p, K^+p and pp collisions, respectively. In all three types of collision, an approximately linear dependence of $\langle n_B\rangle$ on n_F can be observed. The odd-even differences appearing for low multiplicities are due to charge conservation. They cannot be reduced by a stronger cut on diffraction. Linear fits to our data according to (1) give the slope parameters listed in table 1. Within errors, no difference is seen between the three types of hh collision.

In Fig.2 we show, vice versa, the correlation $\langle n_F(n_B)\rangle$. The slope parameter b_F for the linear fits to the data is also given in table 1 and agrees within errors with b_B. For brevity we shall, therefore, use (1a) and omit from now on the subscript F or B on a and b not only for pp collisions, but also for the asymmetric π^+p and K^+p systems.

In Fig.2, the data are compared to three different Monte Carlo models, the single string LUND model [17], a two string dual parton model (DPM) [18] and the two string FRITIOF2.0 model [19]. The same non-diffractive cut has been applied to the models as to the data. In DPM, the two chains are spanned between beam and target (di)quarks. In FRITIOF, one of the chains originates from beam, the other from target excitation by multiple soft gluon exchange. Each of the strings is treated as a quark-antiquark chain (for the meson jet) or quark-diquark chain (for the proton jet) at an energy corresponding to the excitation mass. In the case of LUND and DPM, symmetric LUND fragmentation is used, while in FRITIOF2.0 a multi-gluon radiation mechanism is included. A total of 120.000 Monte Carlo events is generated for each of the three models, so that statistical errors are smaller than those of the data samples by the root of the corresponding ratios.

The single chain LUND model, very successful in describing e^+e^- data, does not follow our data at all. On the other hand, both two chain models predict $\langle n_F\rangle$ to increase with n_B. In particular, the FRITIOF

approach is in agreement with the data, although it is below the data at low multiplicities and the dispersion D of the overall charge multiplicity distribution is not fully reproduced by the model [20].

A comparison of all available results [1,2,5,6,7,8,9] for the slope b in various hh collisions is given in fig.3a. Different cuts have been used in defining the non-diffractive samples. Nevertheless, there seems to be no significant difference between the various types of hh collision. The correlation strength b increases logarithmically with the cms energy $\sqrt{s}$. The highest value so far, b=0.65±0.01, has been measured at $\sqrt{s}$=900 GeV by the UA5 collaboration [2].

The values of the slope b available for lepton-lepton and lepton-nucleon collisions are summarized in fig.3b. The data are from two e^+e^- experiments, one at PETRA and one at PEP [10], from the EMC μp experiment [11] and from a $\nu p(\bar{\nu}p)$ experiment in BEBC [12]. The authors of all four experiments claim to see no significant dynamical F-B multiplicity correlations. Nevertheless, a certain energy dependence is visible and the two highest energy (and smallest error) TASSO points are larger than zero by many standard deviations. So, higher energy will be able to tell.

At this point it is worth stressing, that at lower energies an influence from trivial correlations caused by kinematical constraints, such as phase space limits and conservation of energy, momentum and charge is still important. The authors of ref. [12] have investigated this problem in detail [21] and conclude, that their b-values reflect this effect below W=5 GeV.

As already pointed out in [22], the slope b is directly related to the parameter $1/k$ of the negative binomial fit to the full charge multiplicity distribution. In particular, if no further correlations exist from conservation laws or dynamics, the forward-backward partition of n particles follows a binomial (see also [23]) and the relation is

$$a_B = \frac{\langle n_B \rangle}{1+\langle n_F \rangle/k} \quad , \quad b_B = \frac{\langle n_B \rangle/k}{1+\langle n_F \rangle/k} \quad = a/k \quad . \tag{2}$$

The dotted lines in Fig.3 give b and its energy dependence derived from the energy dependence of $1/k$ [14,24] under the assumption of random partitioning. For hh collisions at high energy, an *anti-correlation* of n_F and n_B develops relative to this assumption. For lh and e^+e^- collisions, the value $b \approx 0$ observed at highest available energies may be accidental and a positive correlation may be expected for $\sqrt{s}$ >30 GeV if $1/k$ keeps inceasing for these types of collision, as well.

Our data allow us to go into more detail in two respects, firstly by restricting ourselves to particles of given charge, in particular to negatives representing only produced particles, and secondly by considering separate (central and off-central) phase space regions, where the influence of conservation laws is smaller.

3.2 Correlations in Separate Charge Combinations

Using the complete non-diffractive sample, the F-B correlations have been determined in full phase space for the different charge combinations (− −), (+ −) and (+ +). These are shown in Figs.4-6, respectively. Linear fit results according to (1a) are given in table 1. No correlations exist at our energy for equal charges in both hemispheres (except for an incident particle effect in (+ +) at $n_F \to 0$), while a particularly strong correlation (b=0.31±0.01) is observed for positive particles going backward and negative particles in the forward region. The same holds for the opposite charge combination (− +) (not shown) with a similar result for the correlation strength b.

Our result may be in contradiction to Chou et al. [25], who introduce a concept of partition temperature in high-energy collisions and who predict equal correlations for the (+ −) and (+ +) combinations, though at much higher energies than ours.

The correlations observed in our data are compared to those expected from LUND, DPM and FRITIOF2.0. The (+ −) combination in Fig.5 is well reproduced by DPM, but slightly overestimated by FRITIOF. It is interesting to note that, contrary to Fig.2, LUND now *shows* a correlation, presumably due to resonance production.

Obviously, the positive correlation of LUND in (+ −) is compensated by the negative correlation for (− −) and (+ +) in Figs.4 and 6, not followed by the data. This de-correlating compensation effect within the LUND chain may be a fundamental problem of this fragmentation picture and a *verification of the effect in e^+e^- data would be extremely useful.*

The DPM Monte Carlo version used [18b] inherits the negative correlation of the LUND chain, but weakened due to the use of two chains. FRITIOF, again, slightly overestimates the correlation and predicts a *positive* slope for (− −).

4. CORRELATIONS IN CENTRAL AND OFF-CENTRAL RAPIDITY INTERVALS

4.1 Central Intervals

In order to investigate in which domain of phase space the correlations are concentrated at our energy, we first determine the F-B correlations in symmetric intervals of different size around y=0. Fig.7 gives the intercept a and the correlation strength b for tracks with $|y| < y_{cut}$ as a function of y_{cut}, for the three data samples. While the intercept a grows linearly with y_{cut} towards a saturation at large y_{cut}, the correlation strength b first increases with increasing y_{cut} towards a maximum around $y_{cut} \approx$1.0 and then decreases towards the full phase space value.

Using (2) to calculate the intercept a and slope b from the negative binomial fits [26] under the assumption of random partitioning, we obtain the dotted lines shown for the pp sample in Fig.7. Except for the very small y_{cut} region, the correlation in y is *weaker* than expected from random partitioning. The anti-correlation with respect to this assumption is much larger in this differential distribution than would be expected from the full phase space behaviour at our energy in Fig.3a.

A similar trend is seen for FRITIOF, but already weaker than in random partitioning. The correlation b is described well in very small intervals, but becomes too large for y_{cut} values above the maximum at y_{cut}=1. LUND and even DPM (using LUND chains) are too weak for all y_{cut} values.

The general trend is the same for the (− −) combination in Fig.8, but now LUND and DPM suffer from the decorrelation effect even stronger than for full phase space in Fig.4. Contrary to the all-charged case, random partitioning is now better than any of the three models. It is a satisfactory decription, except in the region $1 < y_{cut} < 3$, but also there the relative anti-correlation is weaker than in the all-charged case.

The complement of Fig.7 and 8, i.e. the parameters a and b for the particles with $|y| \geq y_{cut}$ is given in Fig.9 and 10, again as a function of y_{cut}. The F-B correlation first decreases with increasing y_{cut} towards a minimum around $y_{cut} \approx$1.0 where b is even negative. Increasing y_{cut} to larger values leads back to positive values of b for all charged particles (Fig.9) and to $b \approx 0$ for (− −) (Fig.10).

The models follow the general trend and the truth seems to be between the two, except that the negative value of b in the minimum at $y_{cut} \approx 1$ cannot be reproduced by either model.

There are very few experiments [1d,2,7,10] explicitely giving F-B correlations in the central region. Two of them, the pp ISR-experiment [1d] and the e^+e^- HRS-experiment [10b] have published results at energies close to our $\sqrt{s}$=22 GeV, so that we can compare.

In Fig.11, the two pp experiments (this exp. and ISR) give rather similar positive values of b for the all charged particle correlation in the region $|y| < 1.0$ ($|\eta| < 1.0$ in case of ISR). In contrast, the e^+e^- experiment does not show any F-B correlation there, at all. For the complementary region $|y| \geq 1$, the slope is close to $b = 0$ in all three cases.

The energy dependence of the correlation strength b in hh collisions for full phase space and for the regions $|\eta| < 1.0$ and $|\eta| \geq 1.0$, separately, is given in Fig.12, using our pp data together with the results from the pp ISR experiment [1d] and the $p\bar{p}$ UA5 experiment [2].

Fig.13 shows the correlation strength b as a function of an increasing gap size $\Delta\eta = 2\eta_{cut}$ in comparison to the ISR [1d] and UA5 [2,27] data, up to the first zero of b. For all energies, b decreases approximately linearly with increasing $\Delta\eta$ and the rate of decrease seems independent of energy. At each energy, the extrapolated intercept, i.e. $\Delta\eta$ positions of b=0, coincides within errors with the corresponding width of the central rapidity plateau. Over this $\Delta\eta$ range, no strong change in behaviour is seen when passing from short range to long range order. Thus, F-B multiplicity correlations are continuously spread over the region of the central rapidity plateau, which widens with ln s.

4.2 Correlations in Off-Central Intervals

A further investigation of the domain of F-B correlations is performed in terms of the left-right right correlation within rapidity intervals of width Δy=2.0, centered around a rapidity $y = y_0$.

The resulting intercept a and slope parameter b are given in Figs.14 and 15 for all charged particles

and for the restriction to negative ones, respectively. There is an asymmetry with respect to y_0=0, due to the fact that the average left multiplicity is taken as a function of the multiplicity of the right half of the interval. Reversing left and right leads to a similar but reversed asymmetry (not shown), just as reversing forward and backward gives similar slopes and intercepts in the central intervals.

The correlation is positive over the central rapidity plateau. At the ends of the rapidity plateau it becomes negative, presumably due to phase-space limitations. Again, we conclude that the left-right correlations are continuously spread over the region of the central rapidity-plateau.

As already observed in Figs.7 and 8 for the central intervals, also here the trend is similar for all charged particles and for negatives, but the effect is weaker in the latter.

All models follow the behaviour in the large $|y_0|$ tails. FRITIOF2.0 can reproduce the behaviour of b over the full range, but underestimates a. DPM, in the other hand, reproduces a, but not the behaviour of the slope b.

5. DISCUSSION WITHIN THE FRAMEWORK OF A GEOMETRICAL PICTURE

In the framework of a simple geometrical picture, a straight forward relation between existing F-B correlations in hh reactions and their absence in e^+e^- collisions is proposed in [13] via eq. (A7) of the Appendix in terms of impact parameters: in this picture the broad hh multiplicity distribution originates from an incoherent superposition of narrow distributions belonging to all possible impact parameters b_i

$$P(n,s) = \int p(n,b_i,s)db_i \cdot weightfunction \quad . \tag{3}$$

The multiplicity distribution for impact parameter $b_i = 0$ is identified with that for e^+e^- collisions. From e^+e^- data at $\sqrt{s}$=29 to 47 GeV [10b and ref. therein] one finds a relative dispersion $(D(n)/\langle n\rangle)^2$= 0.11±0.01, essentially equal to $(\langle d_n(\Delta)\rangle/\langle n\rangle)^2$ [13b], and, therefore, from (A7) a slope $b \approx 0$, in agreement with experiments in the same energy range.

Going within the geometrical picture to hh collisions, one takes $(\langle d_n(\Delta)\rangle/\langle n\rangle)^2$ from e^+e^-. This supported by the fact that the summation over impact parameters according to (3) does not change much the distribution in the variable $\Delta = n_F - n_B$. However, the integration causes a large spread in the overall distribution for the variable $n = n_F + n_B$, thus leading to larger values for the dispersion $D(n)$. From (A7) one then gets for the overall correlation strength

for π^+p : $b = 0.19 \pm 0.04$
for K^+p : $b = 0.21 \pm 0.04$
for pp : $b = 0.20 \pm 0.04$

in reasonable agreement with our values given in table 1.

The experimental observation that the F-B correlations are restricted to the central region can be interpreted in the geometrical picture by the central production not being limited to small impact parameters.

In a recent paper Barshay (last ref. [13b]) tries to extend his model to describe charge separated F-B correlations, both in hh and e^+e^- collisions. He claims that the quantity $d_n^2(\Delta)$ at fixed n must contain dynamical F-B correlations and proposes a general parametrization of that quantity depending on $\langle n\rangle$ and n. A similar attempt is in fact already made by Chou and Yang [13a] who show that the UA5 $p\bar{p}$-data at $\sqrt{s}$=540 GeV [28] follow the simple relation

$$d_n^2(\Delta) = \langle \Delta^2\rangle_n - \langle \Delta\rangle_n^2 = 2n \quad . \tag{4}$$

This is in agreement with Barshay's parametrization within the range of n available at this energy and indicated in Fig.16.

We determine the dependence of $d_n^2(\Delta)$ on n from our data and compare it in Fig.16 with UA5 results, as well as with values at lower energy calculated from published data [6]. While the difference between pp and π^+p data is very small at our energy, an interesting energy dependence is observable between 5.6 and 546 GeV, with slopes as given in table 2. The slope of 2, expected from (4), is only reached at Collider energies and it is approached from below.

6. CONCLUSIONS

1. The forward-backward multiplicity correlation parameter b becomes positive for hadron-hadron collisions at $\sqrt{s}$ ≈5 GeV, while this does not happen until 15 GeV in lepton-hadron and 30 GeV in e^+e^- collisions. The observed F-B correlation is weaker, however, than to be expected from the full multiplicity distribution under the assumption of random partitioning between hemispheres.
2. The correlation observed for all charged particles is due to a correlation in unequal charges (+ −), and absent at our energy in equal charge combinations, (− −) and (+ +).
3. Within small central rapidity intervals $|y| < y_{cut}$, the correlation first increases as a function of the interval size, to reach its maximum strength at $y_{cut} \approx 1$, and then decreases towards the full phase space value. All charged particles are strongly, negatives only weakly anti-correlated relative to random partitioning.
4. Excluding a central region $|y| < y_{cut}$ leads to a decrease towards a negative b minimum, at $\sqrt{s}$=22 GeV centered at $y_{cut} \approx 1$. The y_{cut} position of the first zero of b increases with the width of the plateau, so that $b > 0$ holds until most of the plateau region is excluded.
5. The trend of the correlation effects is reproduced by the FRITIOF2.0 model, but the strength of the effect is, in general, overestimated.
7. The effect is underestimated and the trend often not reproduced by the single LUND chain and even by a DPM version using two LUND chains. A comparison of the various charge combinations in e^+e^- collisions to the non-zero slopes expected for these from LUND would be essential.
8. The geometrical picture has an explanation for the difference in strength of the correlation for e^+e^- and hh collisions, but more definite predictions only seem to be fulfilled at much higher energies.

ACKNOWLEDGEMENT

It is a pleasure to thank the operating crews and staffs of EHS, SPS and H2 beam, as well as the scanning and measuring teams of our laboratories for their invaluable help with this experiment.

We particularly would like to thank S. Barshay and D. Rein for substantial theoretical support and enlightening discussions with respect to the geometrical model.

APPENDIX

Using a straight line fit of the form

$$\langle n_B(n_F)\rangle = a_B + b_B n_F \qquad (A1)$$

to describe F-B multiplicity correlations, the slope b_B is given by

$$b_B = (\langle n_F n_B\rangle - \langle n_F\rangle\langle n_B\rangle)/(\langle n_F^2\rangle - \langle n_F\rangle^2) \quad . \qquad (A2)$$

The nominator is called $\mathrm{cov}(n_F, n_B)$, and the denominator is equal to D_F^2, the dispersion of the forward multiplicity ditribution. The correlation strength is therefore given by

$$b_B = cov(n_F, n_B)/D_F^2 \quad \text{or} \quad b_F = cov(n_F, n_B)/D_B^2 \quad . \qquad (A3)$$

By using $n = n_F + n_B$ and $D^2 = \langle n^2\rangle - \langle n\rangle^2$ the relation between the dispersion in the separate hemispheres and the total dispersion D can be shown to be

$$D^2(n) = D_F^2 + D_B^2 + 2cov(n_F, n_B) \quad . \qquad (A4)$$

In a similar way, by using $d_n^2(\Delta) = \langle\Delta^2\rangle_n - \langle\Delta\rangle_n^2$ as the dispersion for the variable $\Delta = n_F - n_B$ at fixed n, one can derive the relation

$$\langle d_n^2(\Delta)\rangle = D_F^2 + D_B^2 - 2cov(n_F, n_B) \quad . \qquad (A5)$$

By making use of (A4) and (A5) one obtains the expression

$$(D^2(n) - \langle d_n^2(\Delta)\rangle)/(D^2(n) + \langle d_n^2(\Delta)\rangle) = 2cov(n_F, n_B)/(D_F^2 + D_B^2) \quad . \qquad (A6)$$

For symmetric systems like e^+e^- or pp one has $\langle n_F\rangle = \langle n_B\rangle, D_F = D_B$, and the right hand side of (A6) becomes the definition of the correlation strength b in (A3), so that one can write

$$b = (D^2(n) - \langle d_n^2(\Delta)\rangle)/(D^2(n) + \langle d_n^2(\Delta)\rangle) \quad . \qquad (A7)$$

For asymmetric systems as π^+p or K^+p we replace D_F^2 and D_B^2 in (A6) via (A3) and obtain for the right hand side of (A6)

$$2/(1/b_B + 1/b_F) \quad , \qquad (A8)$$

the harmonic average of b_F and b_B.

It has been verified that the values of b determined this way from results on $D^2(n)$ published earlier [26] and $d_n^2(\Delta)$ given in Fig.16 are in good agreement with those determined from (A1) directly (table 1).

REFERENCES

1. For pp collisions:
   a) at 69 GeV/c: France-Soviet Union Collab.: "Study of the inclusive reaction $pp \rightarrow \pi^- + X$ at 69 GeV/c", paper submitted to the Aix-en-Provence International Conference (1973);
   b) at 102 GeV/c: C. Bromberg et al.: Phys. Rev. D9 (1974) 1864;
   c) at 205 GeV/c: T. Kafka et al.: Phys. Rev. Lett. 34 (1975) 687;
   d) at $\sqrt{s}$=24,31,45,53,63 GeV: S. Uhlig et al.: Nucl. Phys. B132 (1978) 15
2. For $p\bar{p}$ collisions:
   at $\sqrt{s}$=200,546,900 GeV: R.E. Ansorge et al.: Z. Phys. C - Particles and Fields37 (1988) 191;
   G.J. Alner et al.: Nucl. Phys. B291 (1987) 445;
   K. Alpgård et al.: Phys. Lett. 123 B (1983) 361
3. A. Capella and J. Tran Thanh Van: Z. Phys. C - Particles and Fields 18 (1983) 85;
   K. Fiałkowski and A. Kotanski: Phys. Lett. 115 B (1982) 425;
   J. Dias de Deus: Phys. Lett. 100 B (1981) 177;
   J. Benecke and J. Kühn: Nucl. Phys. B 140 (1978) 179;
   A. Capella and A. Krzywicki: Phys. Rev. D 18 (1978) 4120
4. P. Carruthers and C.C. Shih: Phys. Lett. 165 B (1985) 209
5. For $\pi^- p$ collisions:
   a) at 40 GeV/c: V.G. Grishin et al.: Sov. J. Nucl. Phys. 43 (1986) 388;
   b) at 200 GeV: J.W. Lämsa et al.: Phys. Rev. D 18 (1978) 3933
6. For $\pi^+ p$ collisions:
   at 8 to 23 GeV/c: H. Grässler et al.: Nucl. Phys. B 90 (1975) 461
7. For $K^- p$ collisions:
   at 110 GeV/c: R. Göttgens et al.: Z. Phys. C - Particles and Fields 11 (1981) 189
8. For $K^+ p$ collisions:
   at 70 GeV/c: V.M. Kubik et al.: Sov. J. Nucl. Phys. 43 (1986) 57
9. A. Wróblewski: Proc. XIVth Int. Symp. on Multiparticle Dynamics, Lake Tahoe (June 1983), edts. P. Yager and J.F. Gunion, (WSPC Singapore, 1984), 573
10. For $e^+ e^-$ collisions:
    a) at $\sqrt{s}$=35 GeV: M. Althoff et al.: Z. Phys. C - Particles and Fields 29 (1985) 347;
    b) at $\sqrt{s}$=29 GeV: M. Derrick et al.: Phys. Rev. D 34 (1986) 3304
11. For $\mu^+ p$ collisions:
    at $4 \leq W \leq 20$ GeV: M. Arneodo et al.: Nucl. Phys. B 258 (1985) 249
12. For νp and $\bar{\nu} p$ collisions:
    H. Grässler et al: " Nucl. Phys. B 223 (1983) 269 and private communication
13. a) T.T. Chou and C.N. Yang: Phys. Lett. B135 (1984) 175; B167 (1986) 453; B193 (1987) 531; Phys. Rev. D32 (1985) 1692; Int. J. Mod. Phys. A2 (1987) 1727;
    b) S. Barshay: Nucl. Phys. B 238 (1984) 277 and Z. Phys. C - Particles and Fields 32 (1986) 513;
    S. Barshay and E. Eich: Phys. Lett. B 178 (1986) 431 and Mod. Phys. Lett. A 1 (1986) 459;
    S. Barshay: Phys. Lett. B 199 (1987) 121
14. M. Adamus et al. (NA22): Z. Phys. C - Particles and Fields 32 (1986) 475
15. M. Bardadin-Otwinowska, M. Szczekowski and A. Wróblewski: Z. Phys. C - Particles and Fields 13 (1982) 83;
    K. Fiałkowski and W. Kittel: Rep. Prog. Phys. 46 (1983) 1283
16. F. Meijers: Ph.D. Thesis, University of Nijmegen (1987)
17. B. Andersson, G. Gustafson, G. Ingelman and T. Sjöstrand: Phys. Rep. 97 (1983) 31
18. a) A. Capella, U. Sukhatme, C.I. Tan and J. Tran Thanh Van: Phys. Lett. 81 B (1979) 68 and Z. Phys. C - Particles and Fields 3 (1980) 329;
    b) M. Adamus et al. (NA22): Z. Phys. C - Particles and Fields 39 (1988) 311
19. B. Andersson, G. Gustafson and B. Nilsson-Almqvist: Nucl. Phys. B 281 (1987) 289 and LUND preprint TP87-6
20. P. van Hal: Ph.D. Thesis, University of Nijmegen (1987);
    A. De Roeck: Ph.D. Thesis, Univeristy of Antwerpen (1988)

21. J.R. Batley: Ph.D. Thesis, University of Oxford (1981)
22. P. Carruthers and C.C. Shih: Phys. Lett. 165 B (1985) 209;
W.A. Zajc: Phys. Lett. B 175 (1986) 219;
A. Białas and A. Szczerba: Acta Phys. Pol. B 17 (1986) 1085 and B 18 (1987) 681
23. D. Zieminska: Phys. Rev. D27 (1983) 502
24. G.J. Alner et al. (UA5): Phys. Lett. 160 B (1985) 199;
M. Arneodo et al. (EMC): Z. Phys. C - Particles and Fields 35 (1987) 335
25. T.T. Chou, C.N. Yang and E. Yen: Phys. Rev. Lett. 54 (1985) 510
26. M. Adamus et al. (NA22): Phys. Lett. B177 (1986) 239;
M. Adamus et al. (NA22): Z. Phys. C - Particles and Fields 37 (1988) 215
27. B. Holl (UA5): Proc. XXI Rencontre de Moriond, Vol. 2, ed. J. Tran Thanh Van (Editions Frontières 1986), p. 223
28. K. Alpgård et al. (UA5): Phys. Lett. 123B (1983) 361

Table 1. Fit parameters

	a_B	b_B	a_F	b_F
all-charged				
π^+p	3.73±0.09*	0.15±0.02	4.04±0.08	0.15±0.02
K^+p	3.74±0.08	0.16±0.02	3.86±0.05	0.15±0.01
pp	3.90±0.09	0.17±0.02	3.56±0.06	0.15±0.01
(− −) combination				
π^+p	1.65±0.01	0.02±0.01		
K^+p	1.65±0.02	0.02±0.01		
pp	1.78±0.03	0.02±0.01		
(+ −) combination				
π^+p	2.21±0.02	0.29±0.01		
K^+p	2.20±0.02	0.31±0.01		
pp	2.29±0.02	0.31±0.01		
(+ +) combination				
π^+p	2.95±0.04	-0.07±0.01		
K^+p	2.96±0.05	-0.07±0.02		
pp	3.00±0.08	-0.07±0.03		

* Errors are multiplied by $\sqrt{\chi^2/NDF}$ if this is larger than unity, mainly due to the odd-even differences.

Table 2. Fit parameters to $d_n^2(\Delta) = \alpha + \beta n$ in Fig.16

$\sqrt{s}$	α	β
π^+p 5.6 GeV [6]	-0.67±0.04	0.86±0.01
π^+p 22 GeV (this exp.)	-2.2 ±0.1	1.44±0.03
pp 22 GeV (this exp.)	-1.4 ±0.3	1.35±0.06
$\bar{p}p$ 546 GeV [28]	0 (fixed)	2 (fixed)

FIGURE CAPTIONS:

Fig. 1: The average number of backward produced charged particles versus the number of forward produced charged particles. The lines are linear fits to the data.

Fig. 2: The average number of forward produced charged particles versus the number of backward produced charged particles. The curves join points predicted by Monte Carlo models for soft hadronic collisions, as indicated.

Fig. 3: Correlation strength b as a function of the cms energy for a) hh collisions, b) for e^+e^- and lepton-nucleon collisions. The dotted lines correspond to the expectation from the energy dependence of the negative binomial parameter $1/k$ under the assumption of random partitioning.

Fig. 4: The average number of backward produced negative particles versus the number of forward produced negative particles. The curves join points predicted by Monte Carlo models for soft hadronic collisions as indicated.

Fig. 5: The average number of backward produced positive particles versus the number of forward produced negative particles. The curves join points predicted by Monte Carlo models for soft hadronic collisions as indicated.

Fig. 6: The average number of backward produced positive particles versus the number of forward produced positive particles. The curves join points predicted by Monte Carlo models for soft hadronic collisions as indicated.

Fig. 7: Intercept a and slope b for all charged particles within the region $|y| < y_{cut}$, as a function of y_{cut}. The curves connect points from models as indicated.

Fig. 8: Intercept a and slope b for negative particles in the regions $|y| < y_{cut}$, as a function of y_{cut}. The curves connet points from models as indicated in Fig.7.

Fig. 9: Intercept a and slope b for all charged particles in the regions $|y| \geq y_{cut}$, as a function of y_{cut}. The curves connect points from models as indicated in Fig.7.

Fig.10: Intercept a and slope b for negative particles in the regions $|y| \geq y_{cut}$, as a function of y_{cut}. The curves connect points from models as indicated in Fig.7.

Fig.11: Direct comparison of F-B correlations in the central region $|y| < 1$ and the complementary outer region $|y| \geq 1$ for experiments at similar energy as indicated.

Fig.12: The correlation strength b as function of the cms energy for different pseudo-rapidity regions indicated.

Fig.13: The correlation strength b as function of an excluded central pseudorapidity gap $\Delta\eta$, for the energies indicated.

Fig.14: Intercept a and slope b for all charged particles in the regions $|y - y_0| < 1$, as a function of y_{cut}. The curves connect points from models as indicated in Fig.7.

Fig.15: Intercept a and slope b for negative particles in the regions $|y - y_0| < 1$, as a function of y_{cut}. The curves connect points from models as indicated in Fig.7.

Fig.16: The quantity $d_n^2(\Delta)$ as a function of n, at the energies indicated. The dotted, dot-dashed and dashed lines are linear fits to the 5.6 GeV π^+p, 22 GeV π^+p and 22 GeV pp data, respectively.

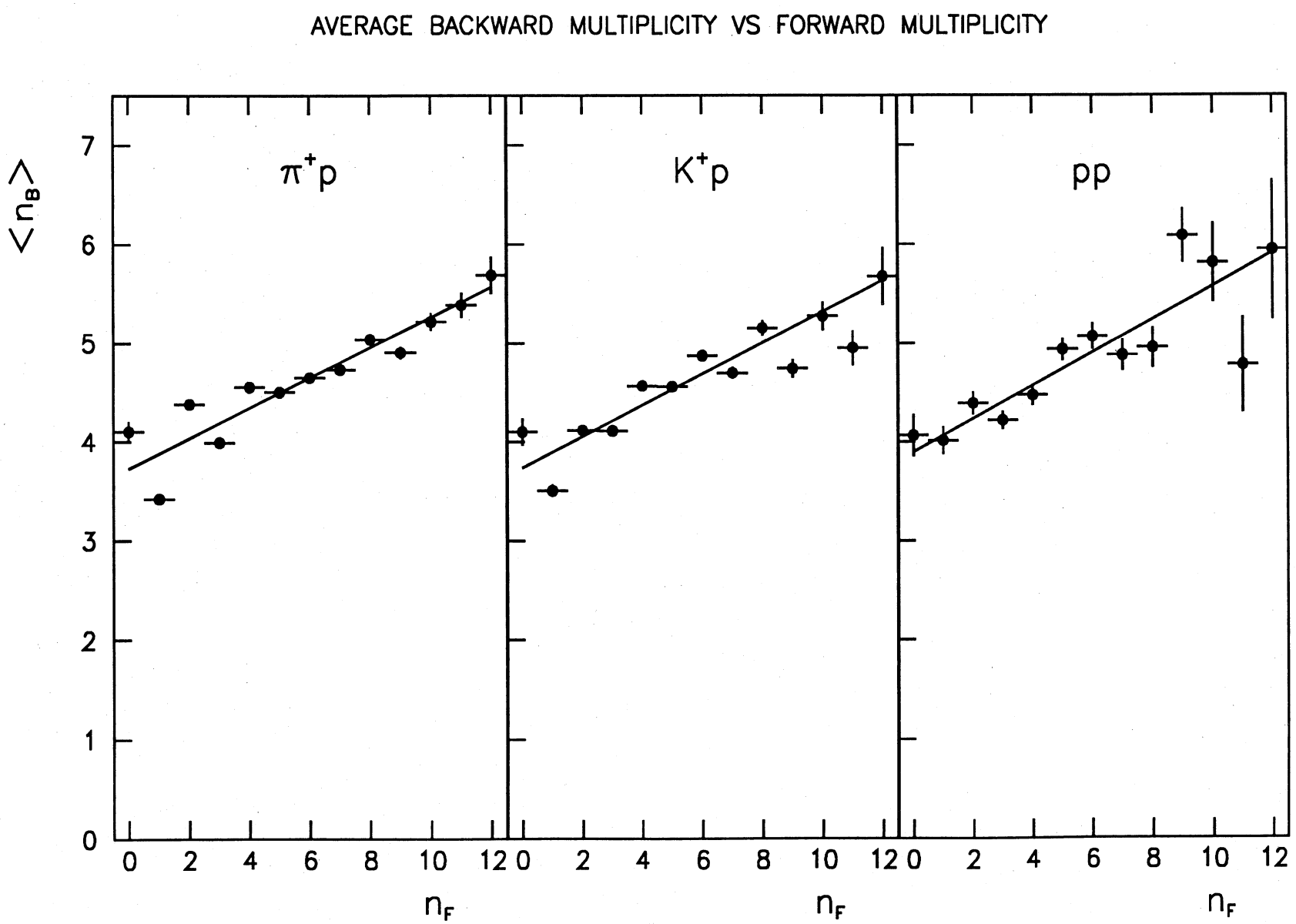
AVERAGE BACKWARD MULTIPLICITY VS FORWARD MULTIPLICITY
$\langle n_B \rangle$
π^+p
K^+p
pp
n_F
n_F
n_F
0
1
2
3
4
5
6
7
0 2 4 6 8 10 12
0 2 4 6 8 10 12
0 2 4 6 8 10 12

Fig.1

AVERAGE FORWARD MULTIPLICITY VS BACKWARD MULTIPLICITY

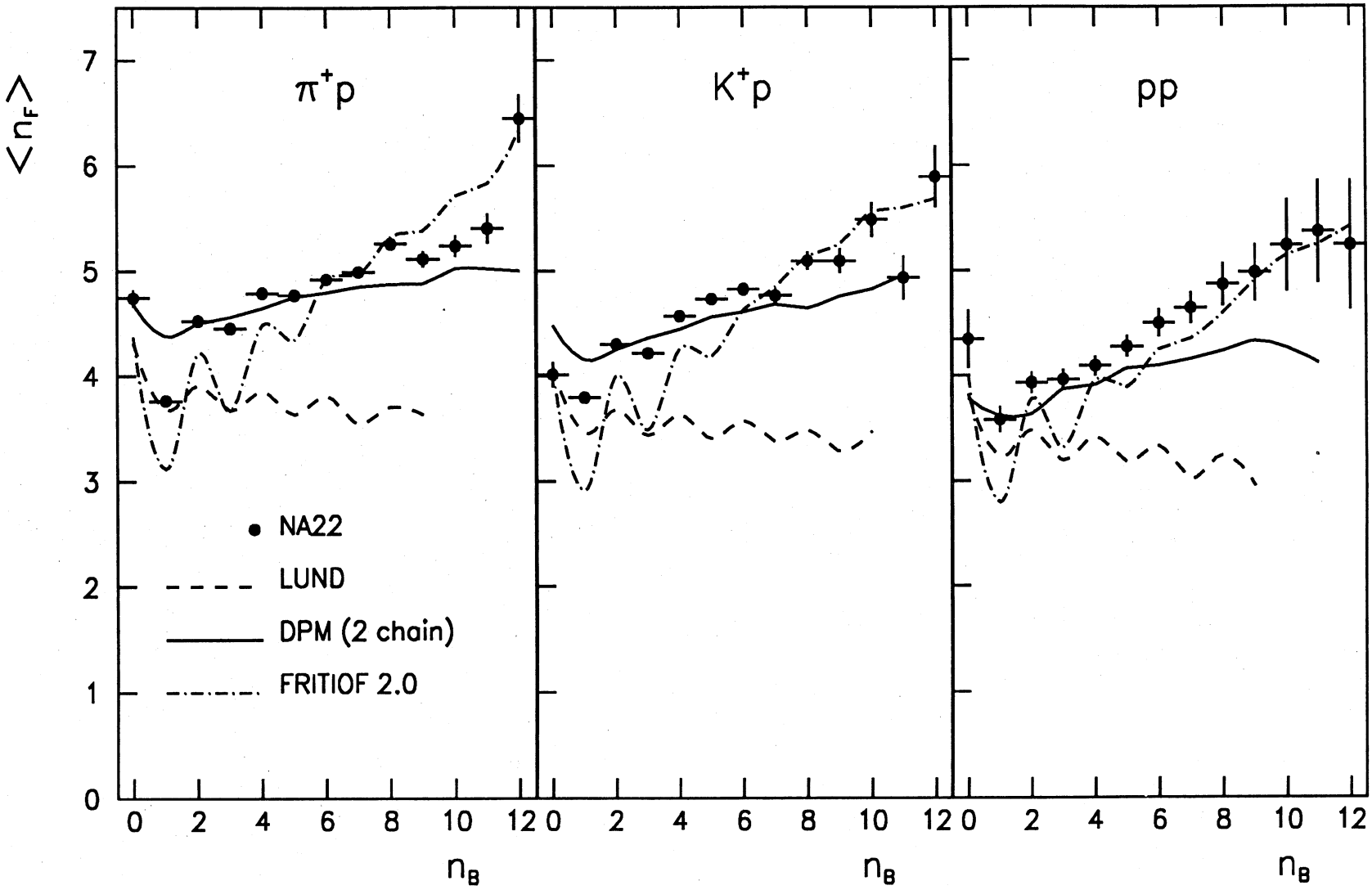

Fig.2

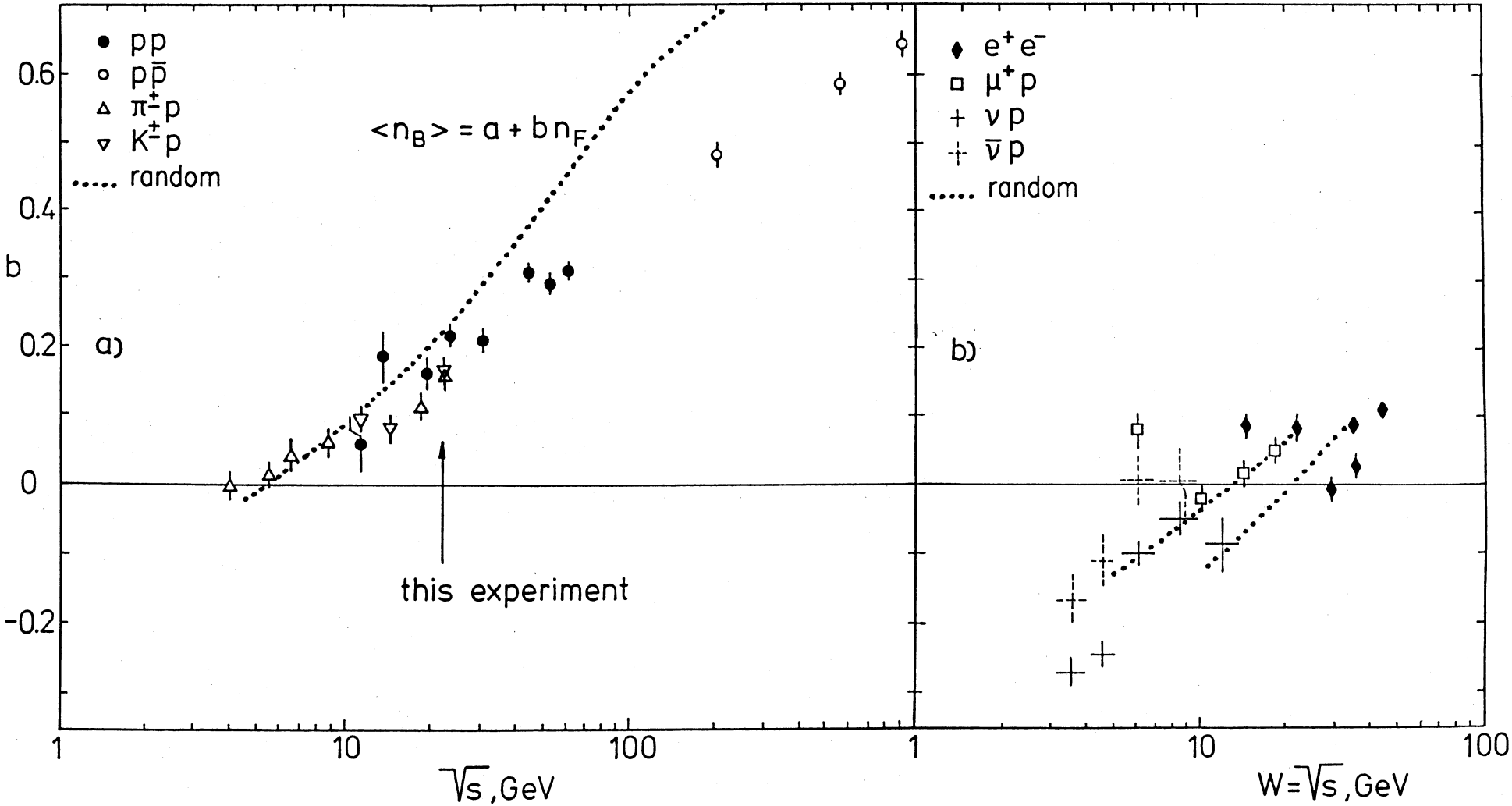
pp
pp̄
π±p
K±p
random
<nB> = a + b nF
a)
b
0.6
0.4
0.2
0
-0.2
this experiment
1
10
100
√s, GeV
e+e−
μ+p
ν p
ν̄ p
random
b)
1
10
100
W=√s, GeV

Fig.3

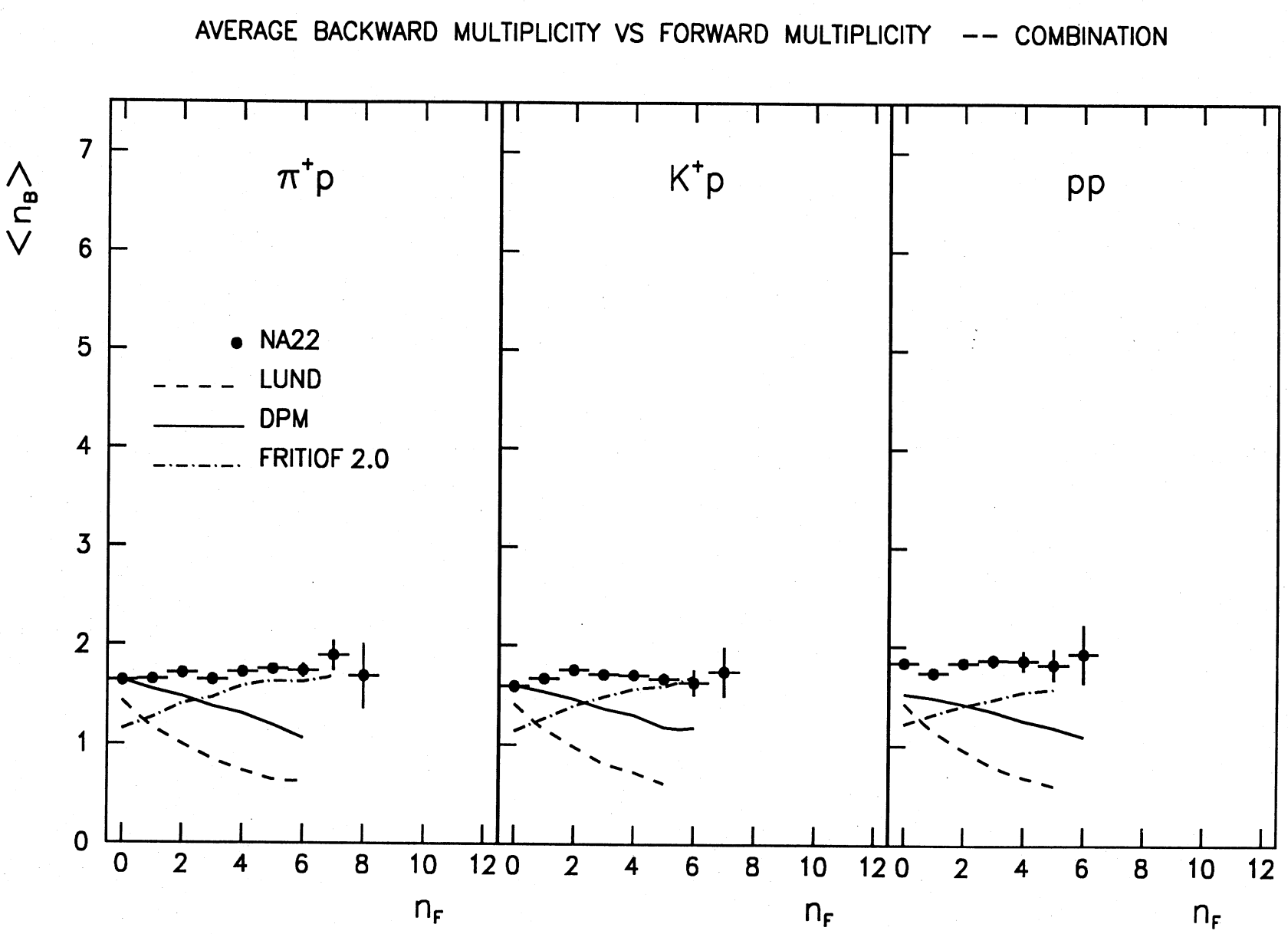
AVERAGE BACKWARD MULTIPLICITY VS FORWARD MULTIPLICITY -- COMBINATION
$\langle n_B \rangle$
$\pi^+ p$
$K^+ p$
pp
NA22
LUND
DPM
FRITIOF 2.0
n_F
n_F
n_F

Fig.4

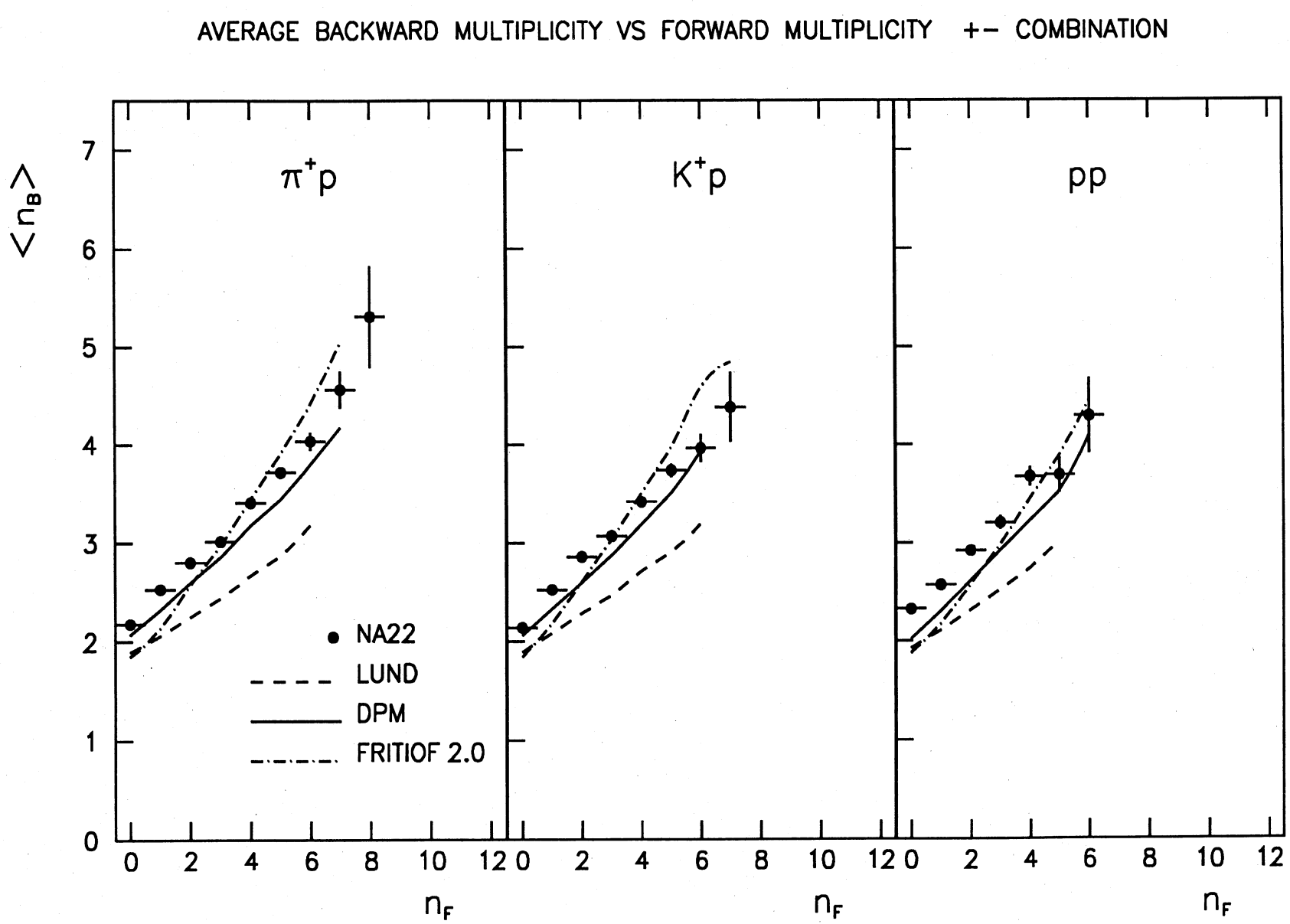
AVERAGE BACKWARD MULTIPLICITY VS FORWARD MULTIPLICITY +− COMBINATION
$\langle n_B \rangle$
π^+p
K^+p
pp
NA22
LUND
DPM
FRITIOF 2.0
n_F
n_F
n_F

Fig.5

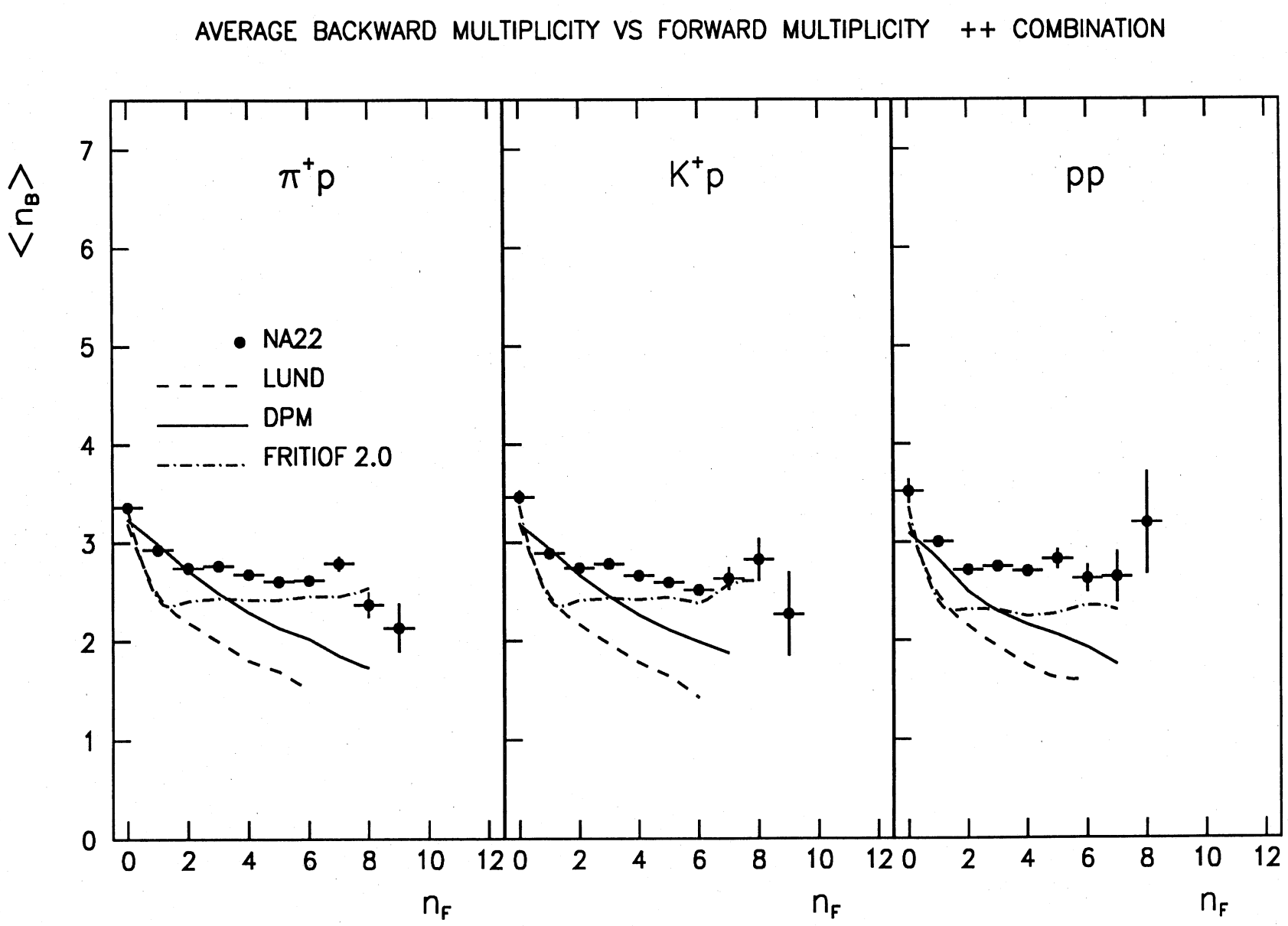
AVERAGE BACKWARD MULTIPLICITY VS FORWARD MULTIPLICITY ++ COMBINATION
$\langle n_B \rangle$
π^+p
K^+p
pp
NA22
LUND
DPM
FRITIOF 2.0
n_F
n_F
n_F

Fig.6

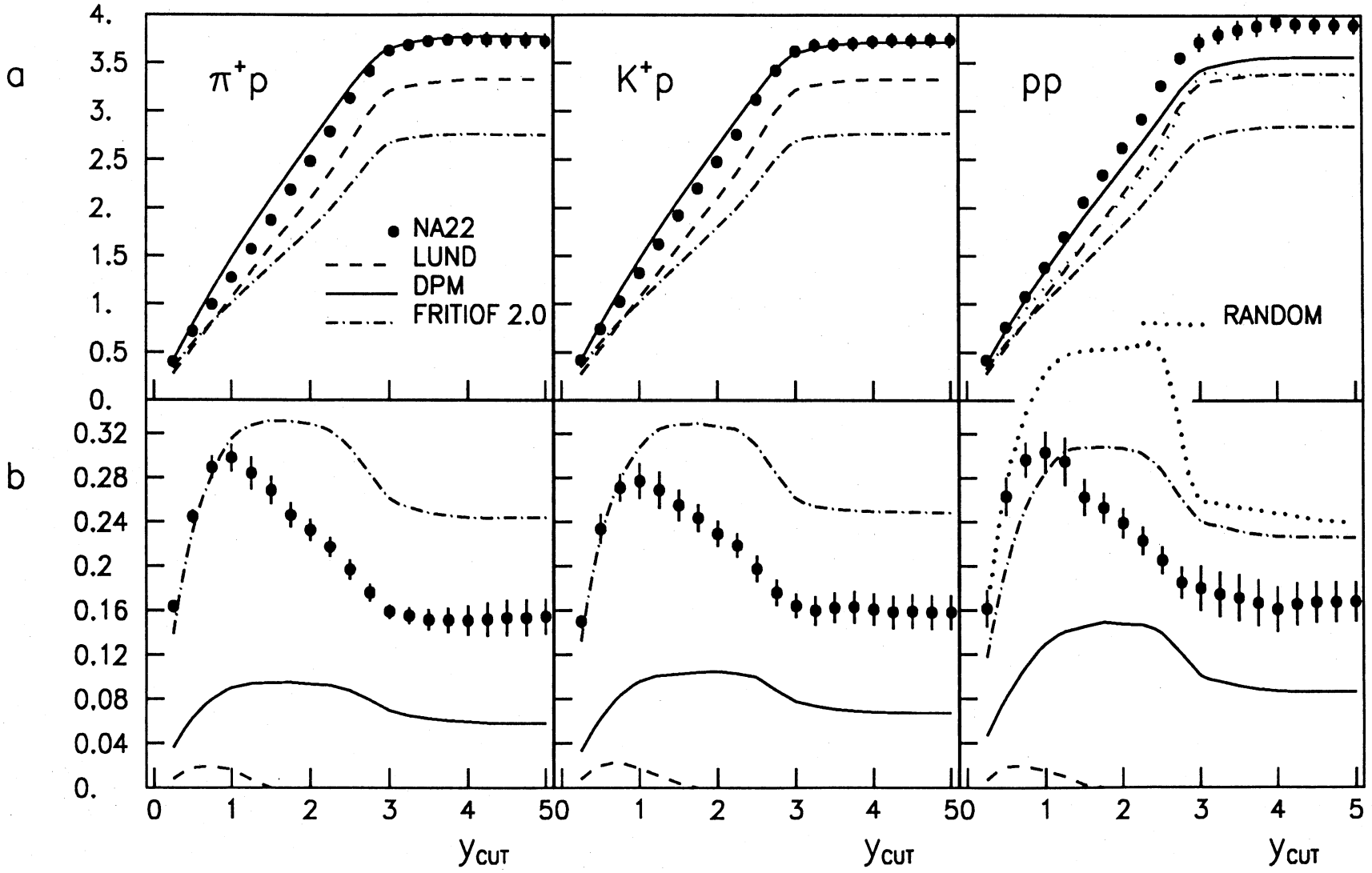
$\langle n_B \rangle = a + b \cdot n_F$ for $|y| < y_{CUT}$, all charged
a
b
$\pi^+ p$
$K^+ p$
pp
NA22
LUND
DPM
FRITIOF 2.0
RANDOM
y_{CUT}
y_{CUT}
y_{CUT}

Fig.7

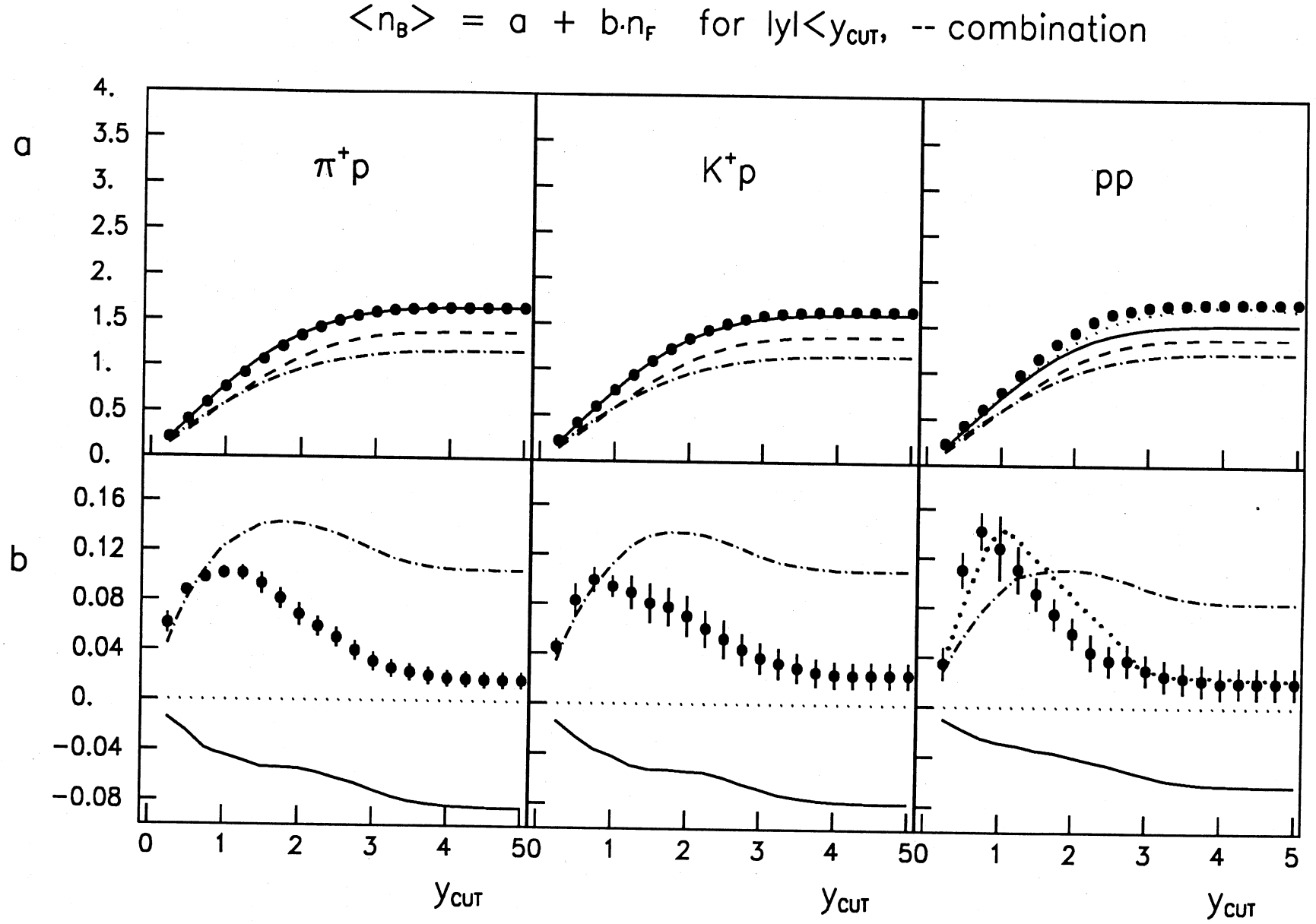
$\langle n_B \rangle = a + b \cdot n_F$ for $|y| < y_{CUT}$, -- combination
a
b
π^+p
K^+p
pp
4.
3.5
3.
2.5
2.
1.5
1.
0.5
0.
0.16
0.12
0.08
0.04
0.
−0.04
−0.08
0
1
2
3
4
50
5
y_{CUT}

Fig.8

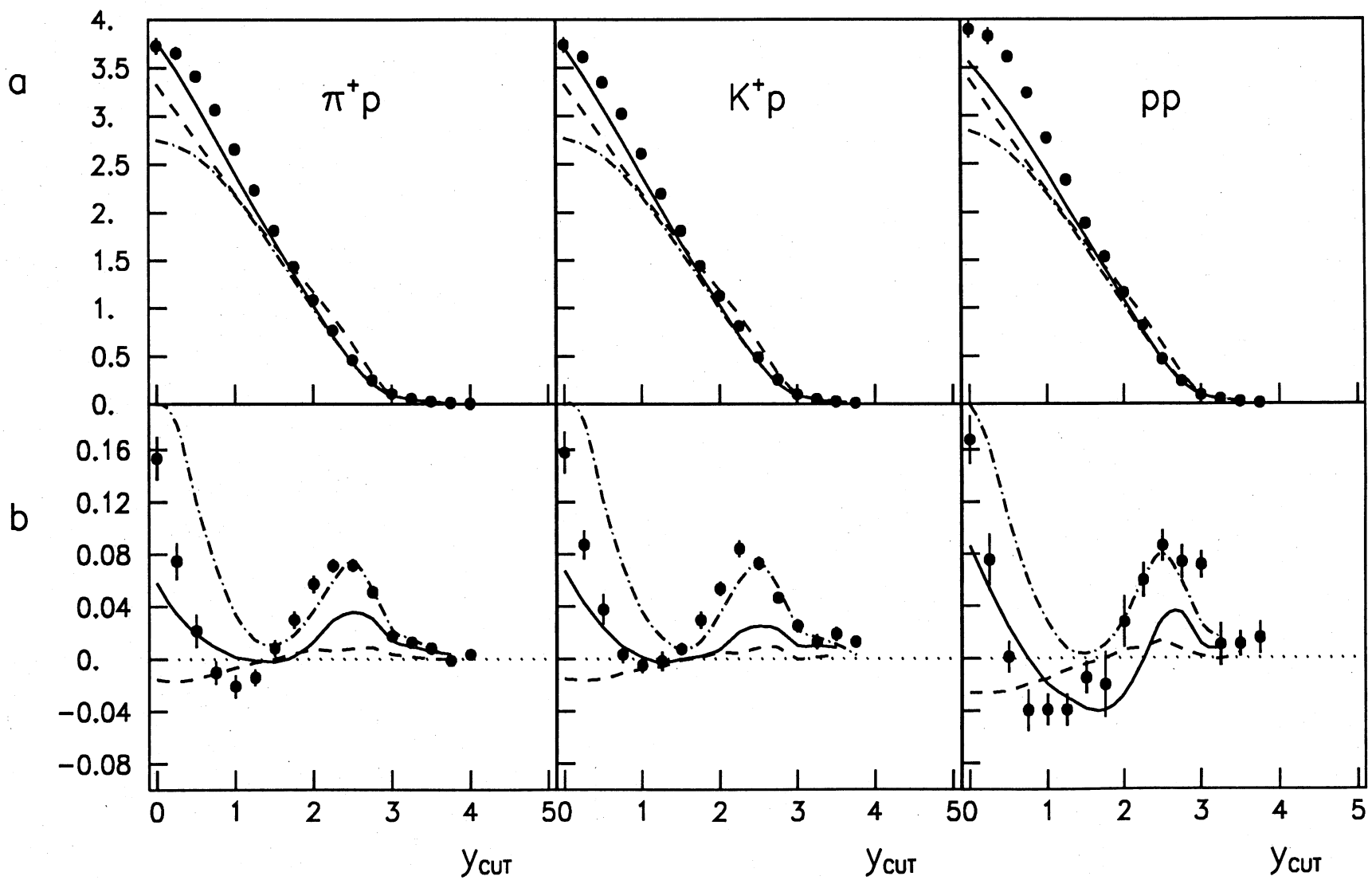
$\langle n_B \rangle = a + b \cdot n_F$ for $|y| \geq y_{CUT}$, all charged
a
b
π^+p
K^+p
pp
y_{CUT}
y_{CUT}
y_{CUT}

Fig.9

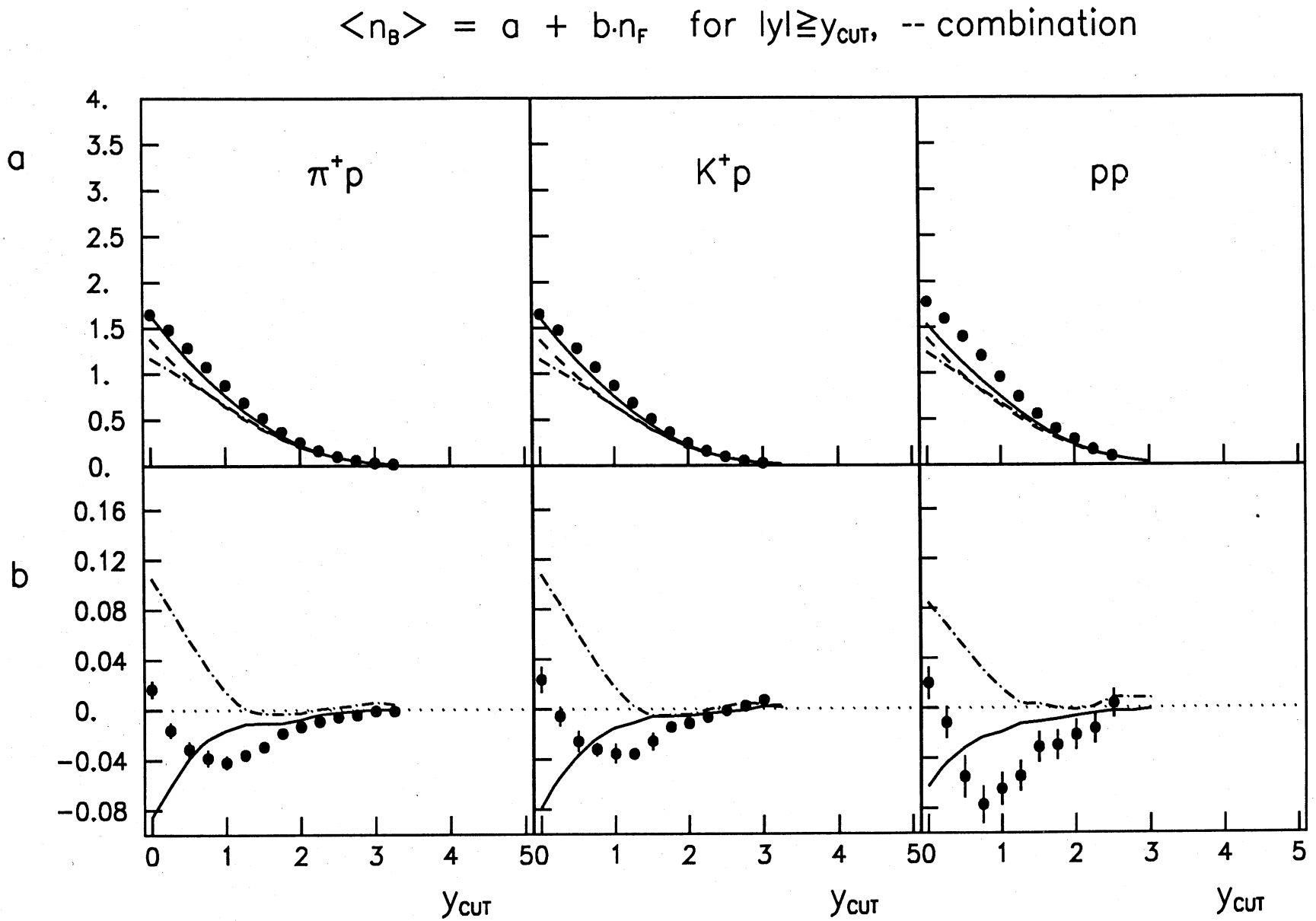
$\langle n_B \rangle = a + b \cdot n_F$ for $|y| \geq y_{CUT}$, -- combination
a
b
π^+p
K^+p
pp
4.
3.5
3.
2.5
2.
1.5
1.
0.5
0.
0.16
0.12
0.08
0.04
0.
-0.04
-0.08
0
1
2
3
4
50
1
2
3
4
50
1
2
3
4
5
y_{CUT}
y_{CUT}
y_{CUT}

Fig.10

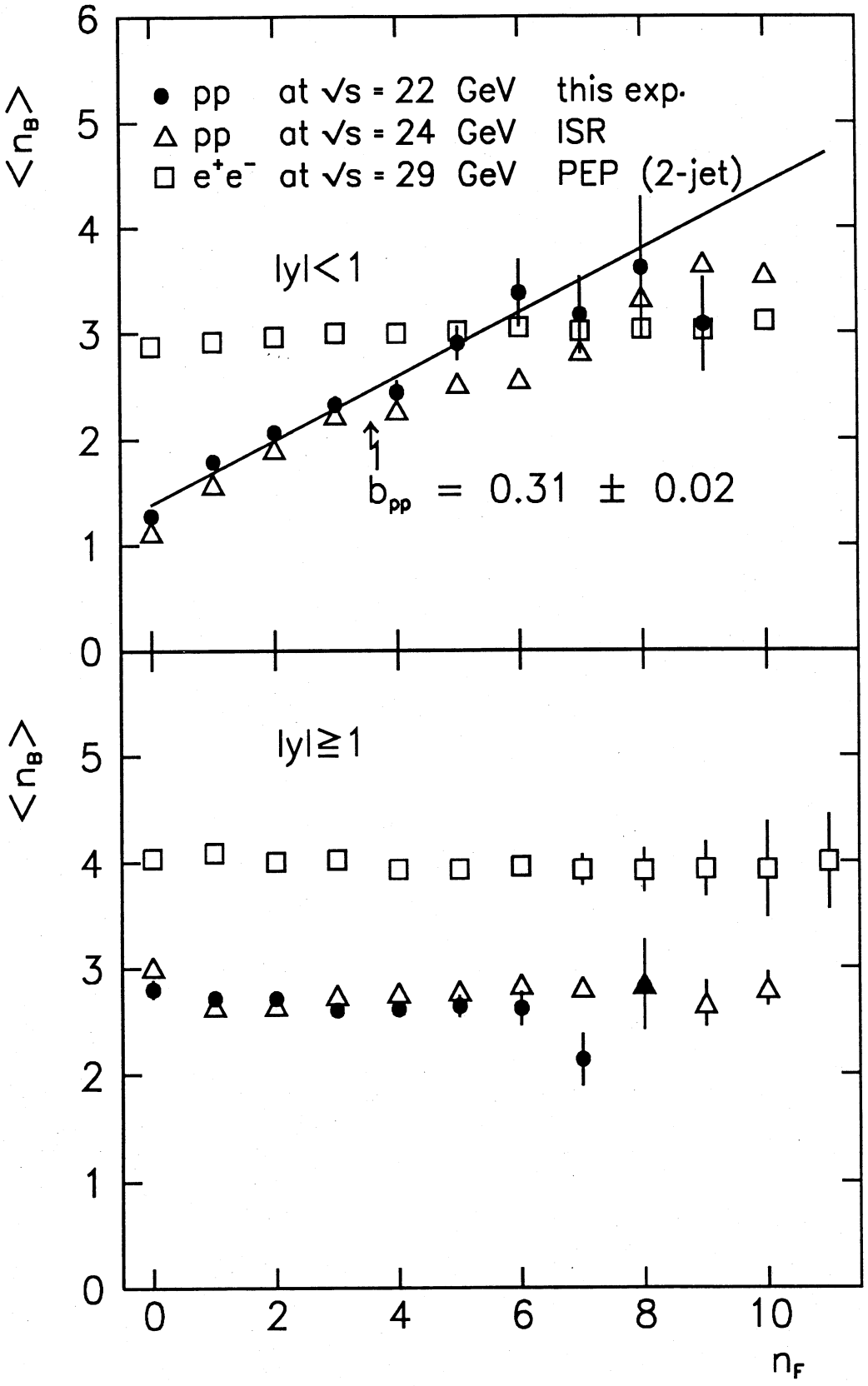
● pp at √s = 22 GeV this exp.
△ pp at √s = 24 GeV ISR
□ e⁺e⁻ at √s = 29 GeV PEP (2-jet)
|y|<1
b_{pp} = 0.31 ± 0.02
|y|≧1
$\langle n_B \rangle$
n_F
0
1
2
3
4
5
6
8
10

Fig.11

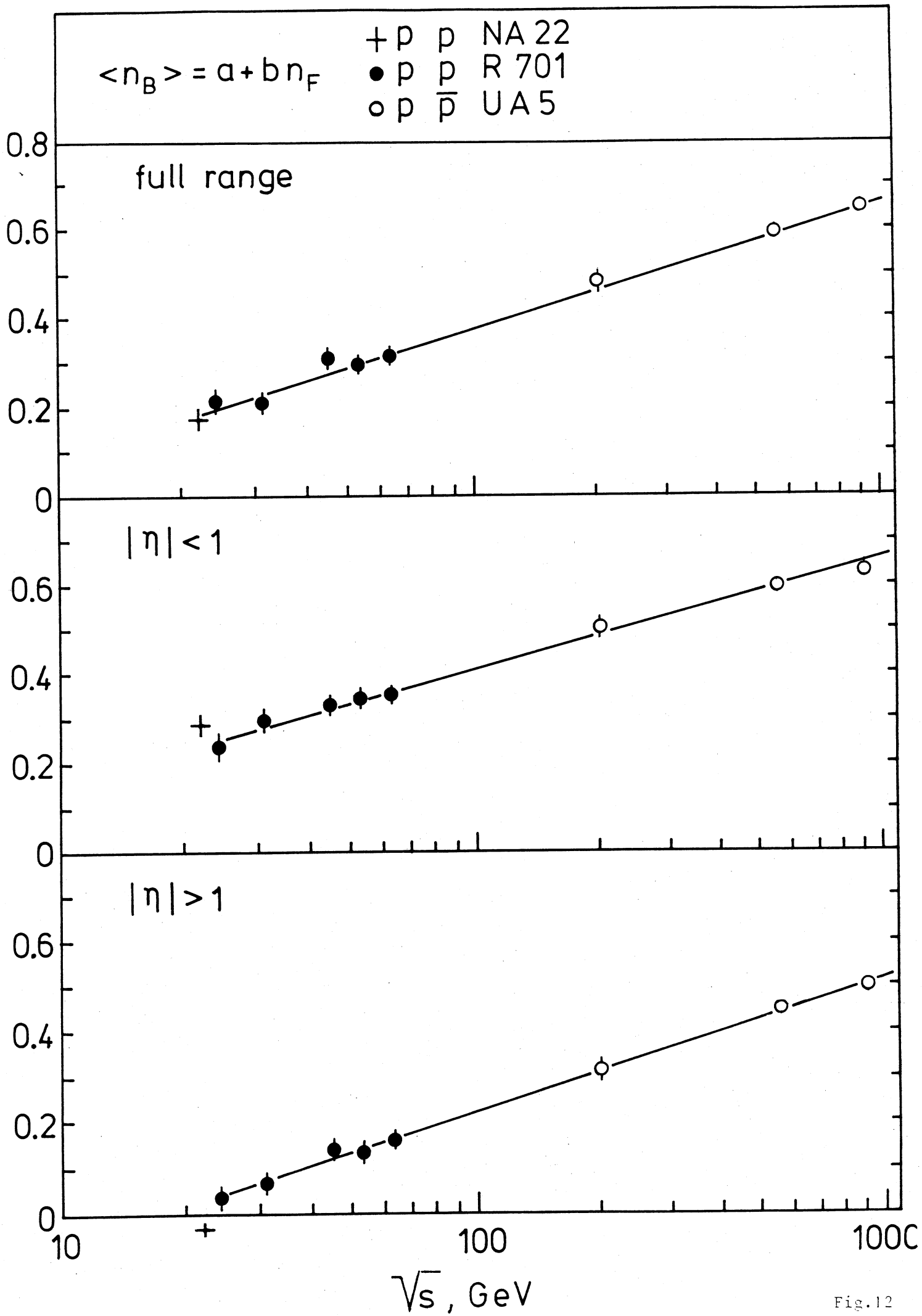
$\langle n_B \rangle = a + b n_F$
+ p p NA 22
● p p R 701
○ p $\bar{p}$ UA 5
full range
$|\eta| < 1$
$|\eta| > 1$
0.8
0.6
0.4
0.2
0
10
100
1000
$\sqrt{s}$, GeV

Fig.12

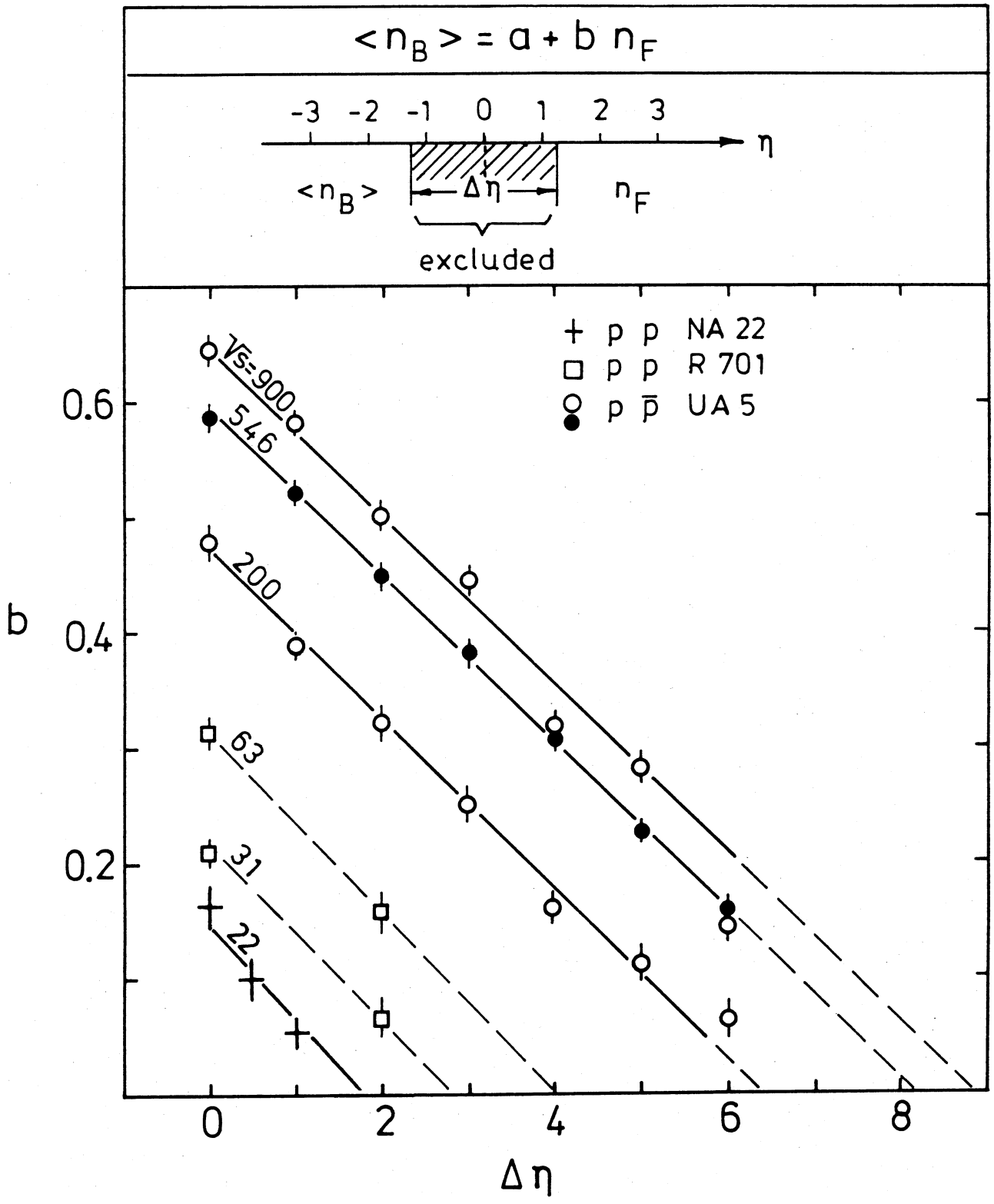
$\langle n_B \rangle = a + b\, n_F$
-3 -2 -1 0 1 2 3
η
$\langle n_B \rangle$
Δη
n_F
excluded
p p NA 22
p p R 701
p p̄ UA 5
√s=900
546
200
63
31
22
b
0.6
0.4
0.2
0
2
4
6
8
Δη

Fig.13

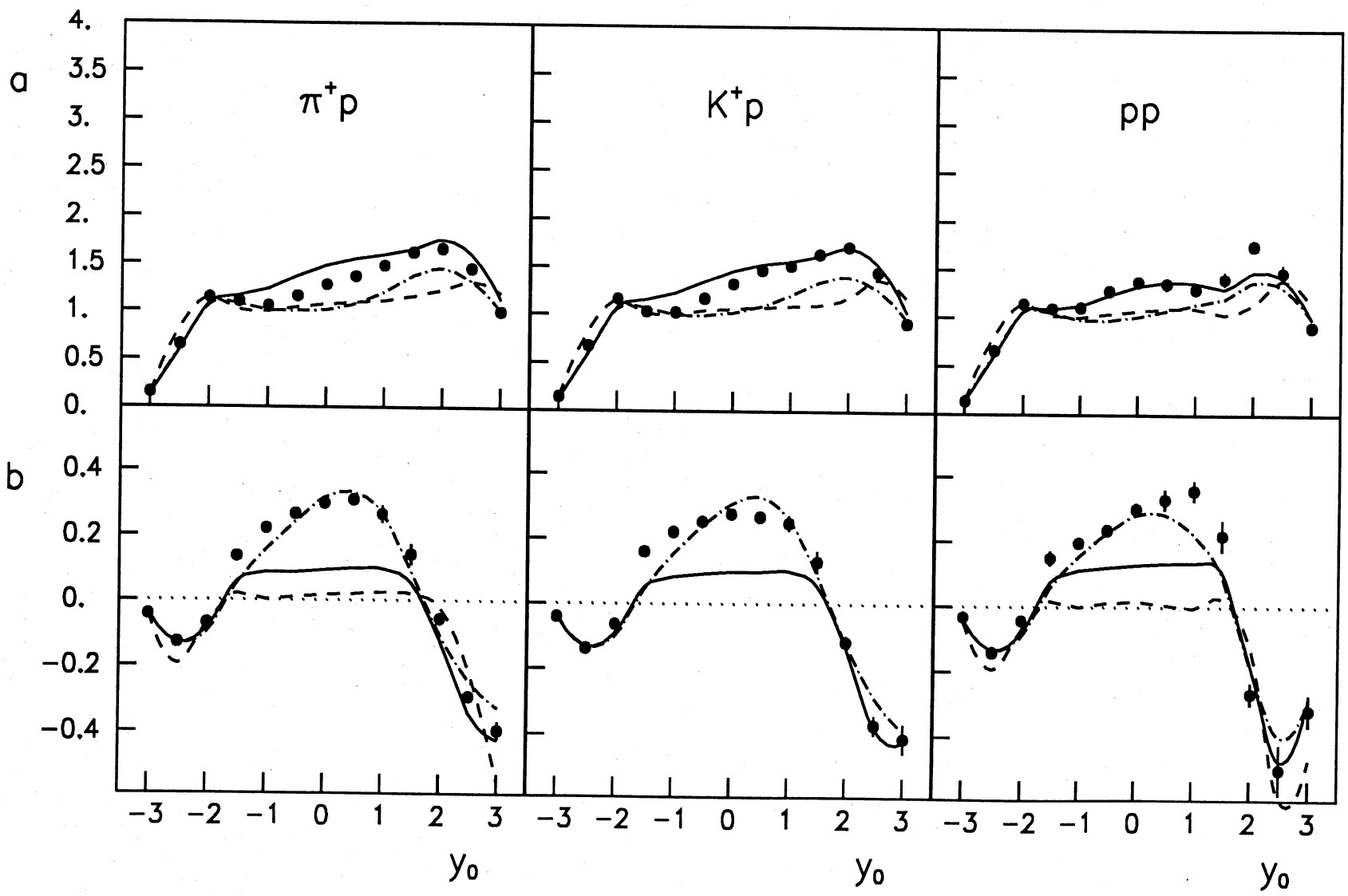
$\langle n_L \rangle = a + b \cdot n_R$ relative to y_0, $|y - y_0| < 1.0$, all charged
a
b
$\pi^+ p$
$K^+ p$
pp
4.
3.5
3.
2.5
2.
1.5
1.
0.5
0.
0.4
0.2
0.
−0.2
−0.4
−3 −2 −1 0 1 2 3
y_0

Fig.14

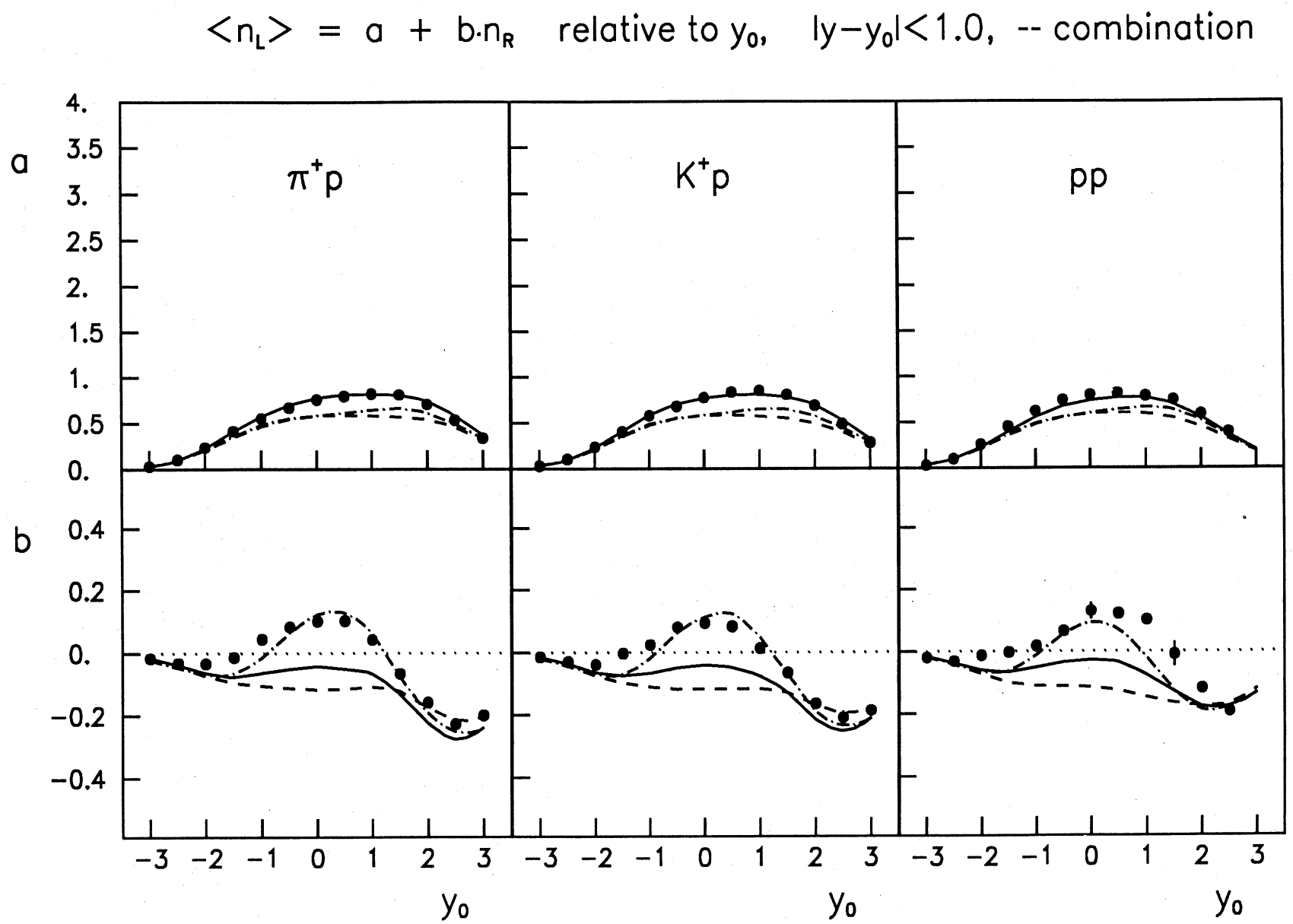
$\langle n_L \rangle = a + b \cdot n_R$ relative to y_0, $|y - y_0| < 1.0$, -- combination
a
b
π^+p
K^+p
pp
4.
3.5
3.
2.5
2.
1.5
1.
0.5
0.
0.4
0.2
0.
−0.2
−0.4
−3 −2 −1 0 1 2 3
y_0

Fig.15

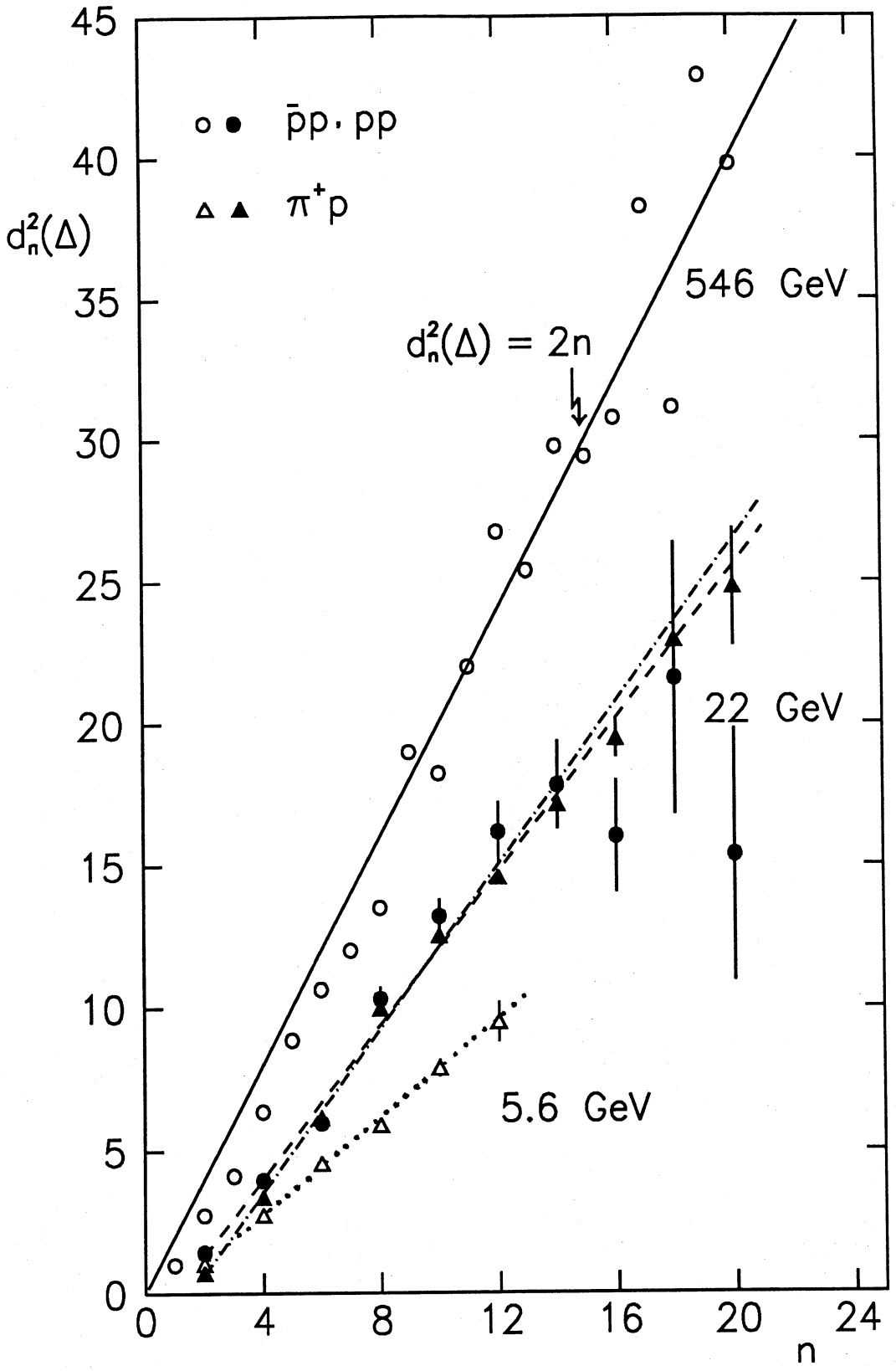
45
40
35
30
25
20
15
10
5
0
0
4
8
12
16
20
24
n
$d_n^2(\Delta)$
$\bar{p}p$, pp
π^+p
546 GeV
$d_n^2(\Delta) = 2n$
22 GeV
5.6 GeV

Fig.16